Phase transition of $(BEDT\text{-}TTF)_3(HSO_4)_2$

Akira Miyazaki, Toshiaki Enoki, Hidehiro Uekusa, and Yuji Ohashi
Department of Chemistry, Tokyo Institute of Technology, Meguro-ku, Tokyo 152 Japan

Gunzi Saito
Department of Chemistry, Kyoto University, Sakyo-ku, Kyoto 606 Japan
(Received 27 August 1996; revised manuscript received 28 October 1996)

The two-dimensional metal $(BEDT\text{-}TTF)_3(HSO_4)_2$ undergoes a metal-insulator transition at 126 K. We investigate the phase-transition mechanism by means of x-ray diffraction, electrical conductivity measurement, electron spin resonance, magnetic susceptibility measurement, and thermal analyses. The transition is first order in nature, whereas no distinguishable change of the crystal structure at the phase transition point is observed, suggesting the minor role of structural change in the transition. Alternatively, this salt behaves as a correlated system in the metallic phase and the transition can be classified as a Mott-type transition caused by the increase of effective on-site Coulomb repulsion originating from anisotropic thermal lattice contraction. [S0163-1829(97)01511-7]

INTRODUCTION

Although many molecular conductors based on bis(ethylenedithio)tetrathiafulvalene (BEDT-TTF) undergo metal-insulator phase transitions, there seems to be no general understanding for the mechanism of their transition. This is because there are many facts to be considered. These salts generally have low dimensionality in their electronic structures, which destabilize their metallic states. The charge-density wave states will appear when the gain of electronic energy become larger than the elastic energy loss caused by lattice modulation. The donor molecule also has high on-site Coulomb repulsion energy (U), which shows features of a highly correlated electron system. If U overcomes the transfer integral t, the Mott-Hubbard transition changes the electronic state from a metallic to an insulating one. Furthermore, since molecular crystals are generally softer than inorganic materials, it is easily assumed that their structural features participate more intensively in their electronic instabilities and phase transitions. Highly anisotropic thermal motion and/or disorder of counteranions and nonplanar six-membered rings fused to a TTF skeleton in crystal structures of various BEDT-TTF salts often contribute to the electronic phase transition, where the order-disorder features are added.

$(BEDT\text{-}TTF)_3(ClO_4)_2$ is one of the examples whose metal-insulator transition mechanism is discussed in detail.[1] In this salt, the partial quenching of the anion rotation, followed by the freezing of the puckering motion of a six-membered ring and displacements of donor molecules, is the motivating force of the transition. This salt belongs to an isomorphous group of $(BEDT\text{-}TTF)_3X_2$ (X denotes a tetrahedral anion). The salts in this group generally undergo metal-insulator transitions, and their transition temperatures depend on the unit cell volume (V_{cell}) of the salt.[2] For example, semiconductive $(BEDT\text{-}TTF)_3(IO_4)_2$ has a large unit cell volume [$V_{cell}=1231$ Å^3 (Ref. 3)], while the above-mentioned $(BEDT\text{-}TTF)_3(ClO_4)_2$ with a smaller unit cell [$V_{cell}=1180$ Å^3 (Ref. 4)] is metallic at room temperature and a metal-insulator transition occurs at $T_{MI}=171$ K. The origin of this trend can be understood qualitatively in terms of the increase in intermolecular transfer integrals caused by the reduction of the cell volume, which stabilizes metallic phases. Nevertheless, the titled salt $(BEDT\text{-}TTF)_3(HSO_4)_2$ (1) has a transition temperature ($T_{MI}=126$ K) that is lower than that of $(BEDT\text{-}TTF)_3(ClO_4)_2$ (2), in spite of its almost equal unit cell volume [$V_{cell}=1179$ Å^3 (Ref. 5)]. Considering the crystal structures of 1 and 2, both of them have a two-dimensional stacking structure with almost the same alignment of donors. The characteristic feature of 1 is the existence of $(OH\cdots O)$-type hydrogen bonds between adjacent HSO_4^- anions. In the crystal of 1, these hydrogen bonds possibly work to restrict the anion rotation, which plays an important role in the phase-transition mechanism in the case of 2. It is therefore interesting to see if this structural difference affects their metal-insulator transition nature. From these viewpoints, we investigated the transition nature of 1 by means of deuterium substitution, electron spin resonance (ESR), magnetic susceptibility, electrical conductivity, thermal analyses, and low-temperature x-ray diffraction and compared the results to those of 2 to discuss the transition nature. Finally, we considered the possibility of a Mott-Hubbard-type transition by estimating the effective on-site Coulomb repulsion as a function of transfer integrals and discussed the mechanism of the phase transition in this context.

EXPERIMENT

BEDT-TTF and BEDT-TTF-d_8 were recrystallized from chlorobenzene. n-$Bu_4N\,HSO_4$ was recrystallized twice from benzene and n-hexane. n-$Bu_4N\,DSO_4$ was prepared by ion-exchange extraction between a toluene solution of n-Bu_4NCl (dried *in vacuo* prior to use) and a D_2O solution of $(C_8H_{17})_3ND\,DSO_4$, which is *in situ* generated from tris(2-ethylhexyl)amine and sulfuric acid–d_2.[6] A characterization of the electrolyte was performed with infrared spectrum. 1,1,2-trichloroethane was treated with concentrated sulfuric acid, dried over K_2SO_4, and then fractionally distilled.

TABLE I. Crystallographic data for 1 at room temperature (RT), 136, 116, and 105 K and for 1-*d* at room temperature.

Compound	1-*h* [a]	1-*h*	1-*h*	1-*h*	1-*d*
temperature	RT	136 K	116 K	105 K	RT
space group	$P\bar{1}$	$P\bar{1}$	$P\bar{1}$	$P\bar{1}$	$P\bar{1}$
a (Å)	9.440(1)	9.375(2)	9.364(1)	9.3809(9)	9.425(1)
b (Å)	16.607(1)	16.493(3)	16.497(2)	16.512(2)	16.58(2)
c (Å)	7.633(1)	7.5108(9)	7.4979(6)	7.4922(4)	7.629(1)
α (deg)	94.97(1)	94.79(1)	94.721(7)	94.716(4)	94.97(1)
β (deg)	96.87(1)	96.43(1)	96.150(7)	96.268(7)	96.91(1)
γ (deg)	87.72(1)	88.060(7)	88.232(3)	88.128(4)	87.70(1)
V (Å^3)	1181.8(3)	1149.3(6)	1147.1(4)	1149.3(3)	1179.0(2)
Z	1	1	1	1	1
No. of observed reflections $[F_O > 4\sigma(F_O)]$	3114	3408	3528	3648	3889
R	0.049	0.051	0.055	0.039	0.040

[a]The unit cell of Ref. 5 is transformed as $\mathbf{a}=\mathbf{b}_0$, $\mathbf{b}=\mathbf{c}_0$, and $\mathbf{c}=-\mathbf{a}_0$.

Single crystals of (BEDT-TTF)$_3$(HSO$_4$)$_2$ (1), (BEDT-TTF)$_3$(DSO$_4$)$_2$ (1-*d*), and (BEDT-TTF-d_8)$_3$(HSO$_4$)$_2$ (1-d_8) were obtained by a galvanostatic ($I=1$ μA) anodic oxidation of donor (1.2 mM) in an argon atmosphere, using n-Bu$_4$N HSO$_4$ or n-Bu$_4$N DSO$_4$ (15 mM) as a supporting electrolyte and 1,1,2-trichloroethane (15 ml) as a solvent. Typical dimensions of the crystals were $1\times2\times0.05$ mm^3.

The dc electric conductivity was measured using a four-probe method ($I=100$ μA) between liquid nitrogen and room temperature. The evaporated gold electrodes ($t=1000$ Å) on the sample were connected to gold wires (20 mmϕ) with gold paint and the temperature was monitored by a Pt thermometer. ESR spectra were recorded down to 5 K with JEOL TE-200 spectrometer, equipped with an Oxford ESR910 continuous-flow helium cryostat. The microwave frequencies were recorded with a frequency counter of the spectrometer and the external field was monitored with a JEOL ES-FC5 NMR field meter. The sample mounted on a Teflon rod using Apiezon N grease was inserted in a 5-mmϕ quartz ESR tube with 20 Torr of He exchange gas. The angular dependence around three axes of the g values and the linewidth are recorded successively at 60 K and 280 K without withdrawing the sample tube from the cryostat in order to ensure the coincidence of the rotational angle between these two temperatures. The accuracy of the angle was within $\pm2°$. The microwave power was limited below 0.5 mW to avoid saturation. Static magnetic susceptibilities were measured at 1 T with a Quantum-Design MPMS-5 superconducting quantum interference device (SQUID) magnetometer, using randomly oriented crystalline samples (5 mg). Specific heats were measured down to liquid-nitrogen temperatures using an ac calorimetric method. The sample was heated by the chopped light (3 Hz) of a halogen lamp and the ac component of the sample temperature was monitored by chromel-alumel thermocouples (25 mmϕ) attached with GE7031 varnish. The typical absolute value of the ac temperature variation was regulated at 10 mK. The temperature of the heat bath was monitored with a Pt thermometer. Differential scanning calorimetry (DSC) measurements were made with a Rigaku TAS300 thermal analyzer equipped with a DSC8230 cooling unit, with 22.5 mg of the sample in the temperature range 90–320 K.

The crystal structure of 1-*d* at room temperature was determined by an x-ray-diffraction method using a Rigaku AFC-7 four-circle diffractometer. The crystallographic data and final reliable factors are summarized in Table I. The absorption effect was corrected using an empirical ψ-scan method, and the structure was solved by direct methods[7] (SHELXS86) then refined by a full-matrix least-squares method (SHELXL93).[8] Hydrogen atoms of donor molecules were attached at geometrically calculated positions, while deuterium was found on a differential Fourier map. To determine the occupancy factors at a disordered site, the thermal parameters for both conformers are restricted to be the same.

The crystal structures of 1-*h* were also determined at 136 K, 116 K, and 105 K, using a Rigaku R-AXIS-CS Weissenberg camera equipped with imaging plates as detectors, and the sample was cooled by the flow of cold, dry, nitrogen gas. The temperature of the sample was calibrated using a chromel-alumel thermocouple. The crystallographic data and final reliable factors are also summarized in Table I. The room-temperature structure[3] was used as an initial structure and then refined by a full-matrix least-squares method (SHELXL93).[8] All of the hydrogen atoms were found on a differential Fourier map and then refined isotropically.

The energy band structures of 1 and 2 at room tempera-

TABLE II. One-centered Coulomb integrals (I) and Slater exponents (ζ) for the Slater-type atomic orbitals.

	S			C		H
Orbitals	3s	3p	3d	2s	2p	1s
$-I$ (eV)	20.0	11.0	5.44	21.4	11.4	13.6
ζ	2.122	1.827	1.5	1.625	1.625	1.3

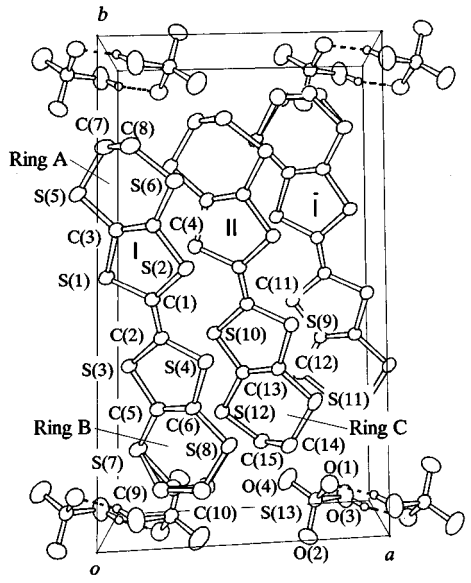

FIG. 1. Crystal structure of 1-*d* viewed along the *c* axis. The numbering scheme of the molecules are also indicated. The dashed lines denote hydrogen bonds between HSO_4^- anions. Hydrogen atoms attached to the ethylene-bridged carbon atoms are omitted for clarity.

ture and low temperature were calculated using a tight-binding method.[9] The coefficients of the highest occupied molecular orbitals (HOMO's) of the donor molecules were calculated using the extended Hückel Hamiltonian according to the Wolfsberg-Helmholz approximation.[10] The basis set consists of Slater-type orbitals of single-ζ quality. The exponents and atomic parameters are summarized in Table II. The overlap integrals S_{ij} between HOMO's of adjacent molecules were then calculated using the same Slater-type basis set and the transfer integrals t_{ij} were estimated at $t_{ij}=ES_{ij}$, where E is the energy level of the HOMO of the donor (-10 eV). The band structures and the shapes of Fermi surfaces are finally obtained from a calculation with the tight-binding approximation.

EXPERIMENTAL RESULTS

Figure 1 shows a unit cell for 1-*d* viewed along the *c* axis at room temperature. Since the unit cell contains one formular unit and one inversion center, there are two crystallographically independent BEDT-TTF molecules. One of them (molecule *I*) is located at general position, while the other (molecule *II*) lies on the inversion center. Molecule *I* is related to molecule *I* by inversion symmetry and these three molecules are stacked along the *a*-*c* direction to form trimerized *I*-*II*-*I* columns. There are many intermolecular side-by-side S$\cdots$S contacts whose distances are shorter than 3.70 Å, i.e., twice the van der Waals radius of the sulfur atom. The shortest ones are S(7)$\cdots$S(11^{i}), 3.408(1); S(5)$\cdots$S(12^{ii}), 3.418(1); and S(6)$\cdots$S(8^{iii}), 3.415(1)Å.[11] These contacts make BEDT-TTF molecules form a two-dimensional layer parallel to *a*-*c* plane. There are three independent six-membered dihydrodithiin rings (rings *A*,*B* for molecule *I*, ring *C* for molecule *II*). Disorder between two conformers, which are the most stable ones in the puckering motion of the six-membered ring, is observed at ring *B*. The occupancies for these conformers are determined as 0.80(1) and 0.20(1), under the constraint that the two conformers have the same thermal parameters. For rings *A* and *C*, conformation is fixed at one conformer and no disorder is observed. DSO_4^- anions are placed between the donor layers. Two anion molecules are related by inversion symmetry and form a dimer via two (OD$\cdots$O)-type hydrogen bonds. The deuterium atom is found near one of the oxygen atoms [O(3)-D, 0.88(6), O(1^{iv})$\cdots$D, 1.76(6) Å].[11] This asymmetry of the hydrogen bond coincides with the bond length of S(13)-O(3) [1.542(3) Å] being apparently longer than that of S(13)-O(1) [1.490(3) Å], which shows that S(13)-O(3) is single bonded, while S(13)-O(1) is double bonded. The O$\cdots$O distance ($d_{O\cdots O}$) at the hydrogen-bonded site is 2.621(4) Å, which is slightly, but significantly, longer than that for (BEDT-TTF)$_3$(HSO$_4$)$_2$ [2.605(5) Å].[5] This result agrees with the empirical rule, which states that the $d_{O\cdots O}$ is generally elongated by approximately 0.02 Å by deuteration when $d_{O\cdots O}$ ranges between 2.60 and 2.62 Å.[12]

On oscillation and Weissenberg photographs at $T=300$, 136, 116, and 105 K, no splitting of Bragg peaks, streaks, or satellite spots are found within the detection limit of the system used. This indicates the good quality of the crystal even at low temperatures and the absence of a superstructure in an insulator phase. Table I shows the comparison of the lattice parameters at low temperatures. The thermal contraction of the *c*-axis length is 2.5 times larger than the contractions of the *a* and *b* axes. Bond lengths at 105 K are generally 0.005–0.01 Å longer than the corresponding values at room temperature.[3] This difference is understood as the effect of the quenching of the intramolecular bending motions. The O$\cdots$O distance at the hydrogen-bonded anion site is 2.631(4) Å at this temperature, which is longer than the corresponding value at room temperature [2.605(5) Å].[5] This

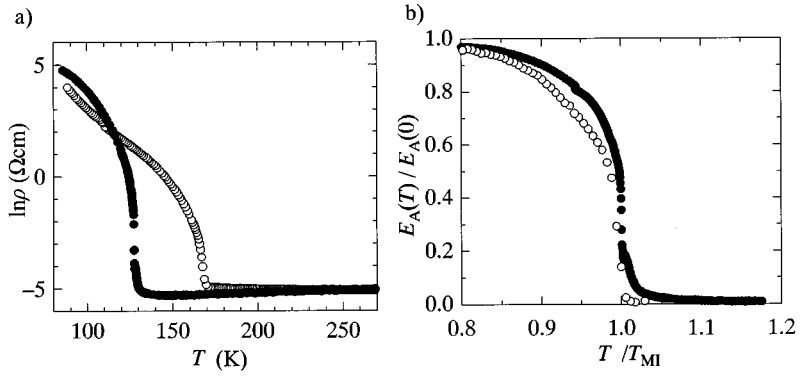

FIG. 2. Temperature dependence of the (a) resistivity and (b) activation energy of 1 (●) and 2 (○). The latter are calculated from dc electrical conductivity as $E_A=k_BT\ \ln[\rho_0/\rho(T)]$, where ρ_0 is the conductivity at 150 K (1) and 190 K (2) and $E_A(0)$ is estimated as 950 K (1) and 1050 K (2), respectively. The results of 2 are cited from Ref. 1.

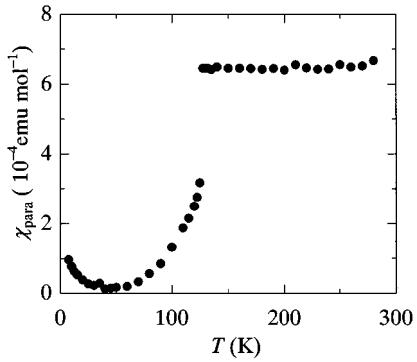

FIG. 3. Paramagnetic susceptibilities plotted against temperature, where the core Pascal diamagnetism contribution (-6.2×10^{-4} emu mol^{-1}) is subtracted from the experimental data.

elongation is again understood as a result of the quenching of anisotropic thermal motion of the S-O bonds. At lower temperatures, no disorder of the six-membered ring is observed. The ethylene bridges at ring *B* are already ordered even in the metallic phase (136 K $\geqslant T_{\mathrm{MI}}$).

The in-plane conductivity of 1 at room temperature is 1×10^{2} S cm^{-1} and a metal-insulator transition takes place at $T_{\mathrm{MI}}=126$ K. Figure 2 shows the temperature dependence of the activation energy E_A for 1 and 2,[1] calculated from the conductivity $\rho(T)$ as $E_A=k_BT\ln[\rho_0/\rho(T)]$, where ρ_0 is the conductivity just above the phase transition regime.[13] The ordinate and the abscissa of the plot are normalized with the phase transition temperature (T_{MI}) and the activation energy at 0 K [$E_A(0)$], respectively. The E_A vs T plot of 2 shows a continuous change around the transition temperature, whereas an abrupt change of the activation energy is observed for 1, which is characteristic of a first-order transition.

In Fig. 3 the paramagnetic component of susceptibility is plotted against temperature, after the core diamagnetic term (-6.2×10^{-4} emu mol^{-1}) is subtracted from the observed data. Temperature-independent Pauli paramagnetic susceptibility is observed above T_{MI}, whose value (6.5×10^{-4} emu mol^{-1}) is nearly equal to that of 2 (6×10^{-4} emu mol^{-1}).[14] At the transition point a sudden decrease of susceptibility occurs, accompanied by an activation-type behavior below T_{MI}. At low temperatures below 50 K, a Curie tail indicates the presence of paramagnetic defects and/or impurities, whose concentration is estimated at 0.2% of the formula unit.

The shape of the ESR signals shows a temperature dependence. In the metallic phase, ESR spectra have asymmetric line shapes when a microwave electric field is applied parallel to the conducting plane (*a*-*c* plane), whereas in the insulator phase the line shapes become Lorentzian. If the electric field of the microwave is applied perpendicular to the conducting plane, a Lorentzian signal is observed in the whole temperature range and line-shape distortion in the vicinity of T_{MI}, as seen in the case of 2,[1] is not observed. The asymmetric line shape is well fitted as a linear combination of the absorption and dispersion contribution of a differentiated Lorentzian curve:

$$\frac{dI(H)}{dH}=-c_1\frac{16x}{(3+x^2)^2}+c_2\frac{3(3-x^2)}{(3+x^2)^2},\quad x=\frac{H-H_0}{\Delta H_{pp}/2}, \tag{1}$$

where H_0 is a center field of the resonance, ΔH_{pp} is a peak-to-peak line width, and c_1,c_2 are the coefficients for both contributions. This asymmetry therefore comes from the skin effect, as a consequence of the high conductivity (10^2 S cm^{-1} at room temperature) and thickness of the sample ($\sim$0.5 mm). Figure 4 shows the temperature dependence of the linewidth and the *g* value obtained by fitting the observed spectrum to the above equation, where the external magnetic field was applied perpendicular to the crystal plane [010], along the direction of crystal elongation (201) and the direction perpendicular to the other two directions [102]. In the metallic phase, the linewidths show an almost temperature-independent value of 5–7 mT, which is almost equal to the value of 2.[15] At the metal-insulator transition point, the linewidths suddenly drop and show an activated-type behavior ($E_A\sim350$ K) just below the transition. Below 50 K the main contribution to the signal comes from defects or impurities, judging from the presence of the Curie tail in the magnetic susceptibility. The *g* values at room temperature for the three directions mentioned above are 2.011, 2.006, and 2.002, respectively, which are characteristic of the principal values for the BEDT-TTF$^{+\cdot}$ cation radical.[16] There is no remarkable change in the vicinity of the transition point, which is quite different from the case of 2,[1] where the large-*g*-value shift ($\Delta g\sim0.03$) is observed around the transition temperature. Figure 5 shows the sinusoidal angular dependences of the *g* value. A comparison of the angular dependence between 60 K and 280 K reveals the absence of the changes in the direction of principal axes associated with the

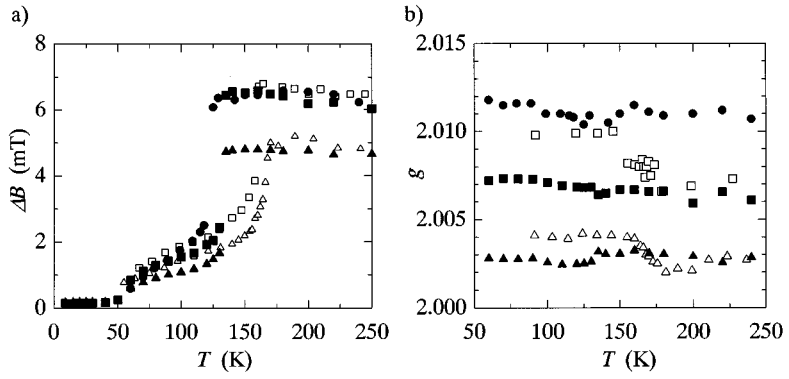

FIG. 4. Temperature dependence of the (a) ESR linewidth and (b) *g* value of 1, where the external magnetic field is applied perpendicular to the [010] plane (●), along the $2a+c$ direction (■), and along the $a-2c$ direction (▲). The corresponding data of 2 are also shown with open symbols for comparison with Ref. 1.

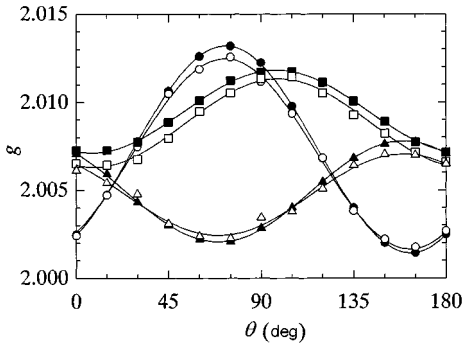

FIG. 5. Angular dependence of the ESR linewidth. The sample rotational axes are the $2a+c$ direction (●, ○, $0°\parallel a-2c$), the $a-2c$ direction (■, □, $0°\parallel 2a+c$), and the normal to the [010] plane (▲, △, $0°\parallel 2a+c$). Filled and open symbols are data recorded at 60 K and 280 K, respectively. Solid lines are fitting curves of $g^2=g_0^2+g_1^2\sin(\theta/2)$.

transition, suggesting that the transition does not change the orientations of the donor molecules.

Figure 6 shows the temperature dependence of specific heat C for 1 and its deuterated compounds 1-d (the anion is deuterated) and 1-d_8 (the donor is deuterated) in the vicinity of the phase transition measured with the ac calorimetric method. There are anomalies at T_{MI} in all the C vs T curves, whose amount is about 10% of the total specific heat. Although the conductivity and magnetic susceptibility show the first-order nature of the transition, the anomaly in the C vs T curve is λ shaped, which is usually observed in a second-order phase transition, suggesting that latent heat accompanied with the transition is quite small. The substitution of the HSO_4^- anion to DSO_4^- raises the transition temperature, but the difference is at most 1 K. The isotope effect is therefore suppressed, which is different from the ferroelectric transition of KH_2PO_4 (123 K)/KD_2PO_4 (213 K),[17] whose origin is the long-range order of the direction of the hydrogen bonds. The isotope effect in T_{MI} between 1-h and 1-d is comparable to the effect of deuteration at ethylene bridge groups (1-d_8), which is also observed in the case of 2-h and 2-d_8.[1] In the DSC measurement, the endothermic peak at the metal-insulator transition point in the heating process is observed, which gives the estimates of the latent heat 170 J mol^{-1} and the transition entropy 0.16R. The presence of the

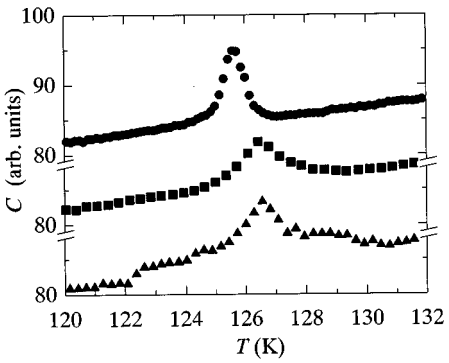

FIG. 6. Temperature dependence of specific heats for 1-h (●), 1-d (■), and 1-d_8 (△).

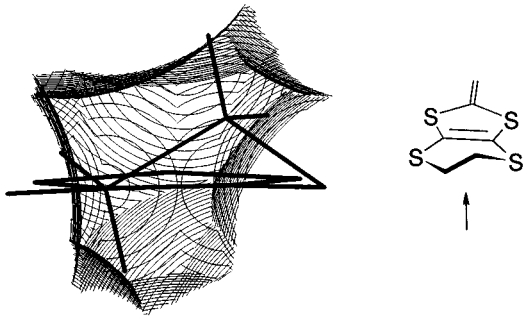

FIG. 7. Cavity for ethylene-bridge group at ring B of 1 at room temperature viewed along the long axis of the molecule. Thick lines shows intramolecular bonds and thin curves are contours drawing in sections separated by 0.05 Å.

latent heat evidences the first-order nature of the transition, in good agreement with the behavior of the conductivity and magnetic susceptibility.

DISCUSSION

Here we first compare the crystal structures of HSO_4 salt (1) and ClO_4 salt (2), which consist of the trimerized I-II-I column and are essentially isostructural for the alignment of donor molecules. As for the disorder at the six-membered rings of donor molecules, one of them (ring B) is disordered for the case of 1, while all of the rings for 2 are ordered, judging from the anisotropy of the thermal parameter for the carbon atoms. It is natural to think that this difference comes from the size and shape of a free space surrounding the ethylene group. In order to discuss this point more quantitatively, we define ''cavities'' for the ethylene groups as follows.[18] We place spheres at the positions of atoms, except those of the ethylene group, where the radius of the sphere is taken as the van der Waals radius of the corresponding atom plus 1.2 Å (the van der Waals radius for the hydrogen atom). A cavity is then defined by the closed space surrounded by the concave surfaces of these spheres. As a typical example, the shape of cavity for ring B of 1 is shown in Fig. 7, in which the boundary for the cavity is expressed as a contour drawing in sections separated by 0.05 Å. The volumes of cavities around the ethylene groups for 1 and 2 at the metallic and the insulator phases are summarized in Table III. All of the cavities for 2 are smaller than the corresponding ones for 1, irrespective of the temperature regions between $T>T_C$ and $T<T_C$. From this result we can say that the ethylene groups in the crystal of 2 is more difficult to pucker

TABLE III. Cavity volumes (Å^3) for ethylene-bridge groups.

Compound	1		2	
Temperature	RT	105 K	RT	120 K
molecule I				
ring A	2.72	2.07	2.43	1.98
ring B	4.41[a]	3.66	3.14	2.70
molecule II				
ring C	3.90	3.19	3.43	2.75

[a]Conformationally disordered.

than those in 1. For the crystal of 1, one of the cavities (ring *B*) is remarkably larger (4.41 Å^3) than the others. This corresponds to the result of the x-ray analysis, which states that only ring *B* is disordered, while the others are not. On lowering the temperature to 105 K, the volume of this cavity decreases down to 3.66 Å^3. Although the threshold value of the cavity volume for the existence of disorder is not obvious, we can say that this shrinkage of the cavity quenches the puckering motion at ring *B* because this volume is smaller than the cavity volume of apparently ordered ethylene bridge sites, such as ring *C* at room temperature (3.90 Å^3).

Next we state how the hydrogen bonds at counteranion sites affect the crystal structures. Comparing mean-square displacements [$U_{\rm eq}=\langle(\mathbf{r}-\mathbf{r}_e)^2\rangle$, where $\mathbf{r}_e$ is the equilibrium position of the atom] of four oxygen atoms of the ClO_4^- anion in crystal 2 at room temperature, one of them has a smaller value (0.069 Å^2) than the others (the average is 0.140 Å^2).[1] This suggests that the ClO_4^- anion rotates with threefold potential minima around the axis on which the former oxygen atom and the chlorine atoms are located. For the case of 1, the mean-square displacement for oxygen atoms is at most 0.073 Å^2 [O(4)], which implies the complete suppression of a rotational motion of anions. This is apparently because of the existence of the hydrogen bonds between HSO_4^- anions, which work to develop the dimerization of the anions. These hydrogen bonds also make the distance between two adjacent HSO_4^- anions in crystal 1 shorter than ClO_4^- anions in crystal 2 [1: S(13)$\cdots$S(13$^{\rm iv}$), 4.169(1) Å;[11] 2: Cl$\cdots$Cl, 4.839 Å]. As a consequence, the interaction between the HSO_4^- anions and ethylene groups is reduced, the cavities for ethylene groups become larger, and the six-membered rings are easy to pucker. It is therefore understood that the existence of hydrogen bonds between anions is the cause of the difference in disordered sites between crystals 1 and 2.

Now we compare the crystal structure of 1 at room temperature and at 105 K. Each intermolecular distance of donor molecules is elongated by 0.005–0.01 Å by lowering the temperature, as a result of the quenching of molecular bending motions. In order to see the charge distribution between the donor molecules, we compared the lengths of the C=C bonds in the TTF skeleton between molecules *I* and *II*. At room temperature, there is no difference in the C=C bond lengths between molecules *I* and *II* [for molecule *I*, C(1)-C(2), 1.368(4); C(3)-C(4), 1.354(4); C(5)-C(6), 1.356(4) Å and molecule *II*, C(11)-C(11$^{\rm v}$), 1.374(4),[11] C(12)-C(13), 1.356(4) Å], suggesting the even charge distribution between molecules *I* and *II*. In the insulator phase, the difference between these bond lengths is still within experimental error [for molecule *I*, C(1)-C(2), 1.371(5); C(3)-C(4), 1.354(5); C(3)-C(4), 1.345(5) Å and for molecule *II*, C(11)-C(11$^{\rm v}$), 1.381(5);[11] C(12)-C(13), 1.360(5) Å]. Therefore, charge separation in the low-temperature phase cannot be observed from the x-ray results. A recent report on infrared spectroscopy[19] shows that the charge separation appears at the phase transition point; namely, below $T_{\rm MI}$, a new absorption appears at 1425 cm^{-1}, which is assigned as the ν_{27} (b_{1u}) mode coupled to the intermolecular charge transfer. This change is explained by modifications of the charge distribution caused by the phase transition.

There are a number of S$\cdots$S contacts between two molecules contacted along the side-by side direction, many of which are closer than twice the van der Waals radii for the sulfur atom (= 3.70 Å) even at room temperature. The most remarkable ones are S(7)$\cdots$S(11$^{\rm i}$) [3.408(1) Å], S(5)$\cdots$S(12$^{\rm ii}$) [3.418(1) Å], and S(6)$\cdots$S(8$^{\rm iii}$) [3.415(1) Å]. At 105 K the distances of these contacts become 3.378(1), 3.410(1), and 3.375(1) Å, respectively, which are approximately 1% shorter than the corresponding values at room temperature. We also define the least-squares plane of the TTF skeleton for each molecule and compare interplanar distances. At room temperature, the distances between molecules *I* and *I*, and between *I* and *II* are 3.761(3) and 3.731(3) Å, respectively. On lowing the temperature to 105 K, these values are reduced to 3.667(4) and 3.664(4) Å, respectively, which are 2.5% shorter than the corresponding values at room temperature. From these result we can say that the thermal contraction is mainly due to intermolecular contacts and the relative contraction is 2.5 times larger for the direction of donor molecule stacking than the direction of side-by-side contacts. This result is consistent with the observed anisotropy of the thermal contraction of the cell parameters ($\Delta c/\Delta a\approx 2.5$).

Here we discuss the transition nature of 1. The results of dc electrical conductivity, magnetic susceptibility, and ESR measurements show that the metal-insulator transition of 1 at 126 K is classified as a first-order phase transition in nature, which is confirmed by the existence of the latent heat. In contrast, for the case of 2, both the ESR linewidth[1] and the magnetic susceptibility[15] gradually change in the vicinity of the phase transition temperature as a consequence of the second-order nature of the transition. We can say, for the following reasons, that the main cause of the transition of 1 is *not* a structural change at the transition point. (i) The space group (triclinic, $P\bar{1}$) remains unchanged between the metallic and the insulator phases and there are no superstructures nor abrupt changes of the lattice constants at the phase transition point. In other words, there is no symmetry breakdown accompanied by the phase transition. (ii) No significant change of the ESR *g* value is observed, showing that the relative orientation of the donor molecule to the crystal remains unchanged in the region of the phase transition. This is completely different from the result for 2, in which the *g* values gradually changes with the amount of $\Delta g\sim 0.03$ as the phase transition occurs.[1] (iii) The hydrogen bonds are asymmetric and are ordered even at the high-temperature phase. This is also supported by the fact that the deuteration at anion sites changes the phase transition temperature little (<1 K). If the ordering of hydrogen bonds were the origin of the phase transition, a large isotope effect would be observed. (iv) Since the conformational disorder at one of the three six-membered rings of BEDT-TTF molecules, which is observed at room temperature, is totally quenched above the transition temperature (at 136 K$>T_{\rm MI}$), there is *no* direct relation between the ordering of the ethylene bridge and the metal-insulator transition.

We can also discuss this point again through the energy band structure calculation using extended Hückel and tight-binding methods since the results of the calculation based on these approximations are affected mainly by the crystal structure of the salt. First, we calculate overlap integrals between adjacent molecules shown in Fig. 8, whose results are

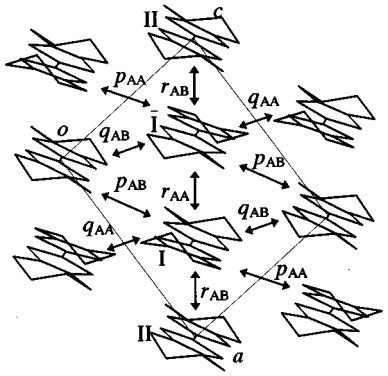

FIG. 8. Schematic drawing of donor molecule arrangement, including symbols for overlap integrals. The origin is shifted to the center of the central C=C bond of molecule II for convenience of calculation.

summarized in Table IV. Overlapping along the $a+2c$ direction (q_{AA},q_{AB}) dominates to the other overlappings for both salts. For the ClO_4 salt (2), one of the side-by-side interaction (q_{AB}) is reduced by half when lowering the temperature below T_{MI}, which is consistent with the molecular orientation change observed with the gradual change of the ESR g value in the vicinity of the phase transition.[1] On the contrary, no such drastic change of transfer integral is observed for 1 between room temperature and 105 K, in good agreement with the experimental result showing the absence of the g-value shift around T_{MI}. The energy dispersion curves and the Fermi surfaces calculated for both salts are illustrated in Fig. 9. At room temperature, both of these salts are classified as semimetals; there are a hole pocket at $\Gamma=(0,0,0)$ and an electron pocket at $Z=(0,0,c^*/2)$. The sizes of the pockets are larger for 1 than 2, which might be the result of a small anisotropy of overlap integrals for salt 1. On lowering the temperature, the Fermi surface of 2 vanishes as the phase transition occurs. The origin of this disappearance comes from the reduction of the side-by-side interaction (q_{AB}). The phase transition for the ClO_4 salt is therefore characterized as a semimetal to band-insulator transition, whose mechanism can be explained by the structural change, especially by the orientational change of donor molecules. On the contrary, the Fermi surfaces for HSO_4 salt survive at 105 K, which conflicts with the experimental results of the semiconductive behavior. The discrepancy confirms that the phase transition is not directly related to the structural change of the salt, such as the orientational change of donor molecules as observed in the case of ClO_4 salt.

TABLE IV. Overlap integrals ($\times 10^{-3}$) calculated for (BEDT-TTF)$_3$(HSO$_4$)$_2$ (1) and (BEDT-TTF)$_3$(ClO$_4$)$_2$ (2).

Compound	1		2	
Temperature	RT	105 K	RT	120 K
p_{AA}	−7.49	−7.96	−4.90	−5.65
p_{AB}	−8.37	−8.64	−6.46	−7.46
q_{AA}	18.74	20.23	21.62	21.92
q_{AB}	14.47	16.14	15.94	8.48
r_{AA}	−3.51	−3.79	−2.21	−2.97
r_{AB}	3.57	3.38	2.97	0.44

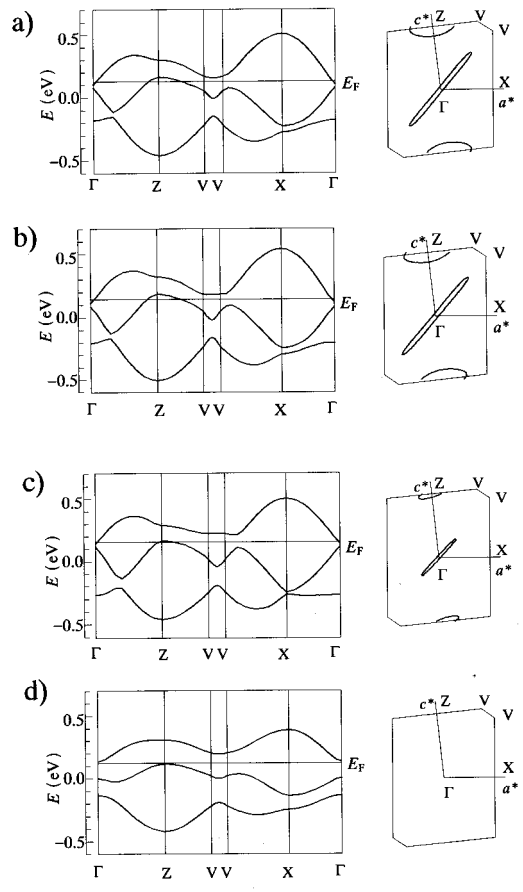

FIG. 9. Band structures and Fermi surfaces for (a) 1 at room temperature, (b) 1 at 105 K, (c) 2 at room temperature, and (d) 2 at 120 K. The origin of the vertical axes are the HOMO energy level of BEDT-TTF. The horizontal lines denote the location of the Fermi level E_F.

We therefore discuss the possibility of the electronic contribution to the phase transition of 1. The relation between the Pauli paramagnetic susceptibility χ_{Pauli} and the entropy for the conduction electron S_{el} is expressed as

$$S_{\text{el}}=\frac{\pi^2}{3}k_B^2 D(E_F)T=\frac{\pi^2}{3}\left(\frac{k_B}{\mu_B}\right)^2\chi_{\text{Pauli}}T, \qquad (2)$$

where $D(E_F)$ is the density of states at the Fermi energy, k_B is the Boltzmann constant, and μ_B is the Bohr magneton. From the estimated value of the Pauli paramagnetic susceptibility (6.5×10^{-4} emu mol^{-1}), S_{el} is calculated as $0.72R$ at the transition temperature, which is 4.5 times larger than the observed entropy change at the transition ($0.16R$). A possible explanation for this difference is that not all of the conduction electrons disappear at the phase transition point, but that there are thermally excited electrons just below the transition points. This assertion is consistent with the activation-type behavior of the susceptibility and ESR intensity data below the transition temperature.

Since the donor molecules form a two-dimensional metallic layer in the a-c plane, the Pauil paramagnetic susceptibility is expressed as

$$\chi_{\text{Pauli}}=\frac{\mu_B^2 N_A}{\pi t} \tag{3}$$

if the electron correlation is neglected, where μ_B is the Bohr magneton, N_A is Avogadro's number, and t is a transfer integral between molecules in the sheet, which is estimated from the overlap integrals at 0.1 eV on average. The observed value $\chi_{\text{Pauli}}=6.5\times10^{-4}$ emu mol^{-1} is considerably large in comparison to the value 1.0×10^{-4} emu mol^{-1} estimated from Eq. (3). This proves the importance of the electron correlation originating from a large on-site Coulomb energy. Judging from these results, the energy band structure calculation performed above is inadequate, especially in the sense of completely neglecting on-site Coulomb repulsion between electrons.

Here we discuss the electron correlation effect on the basis of the crystal structure of 1 with of *I-II-I* triads, taking account of on-site Coulomb repulsion on the donor molecules. We adopt the Hubbard Hamiltonian for the triad with the on-site Coulomb repulsion U and the intratrimer transfer integral t and, by solving the Hamiltonian analytically, we obtain the ground-state energies $E(n)$ for one-, two-, and three-electron states as

$$E(1)=-\sqrt{2}|t|,$$

$$E(2)=\frac{1}{3}\{U-\text{Re}[(1-\sqrt{3}i)A]\},$$

$$E(3)=\frac{2}{3}(U-\text{Re}A), \tag{4}$$

where

$$A=[U^3+9Ut^2+\sqrt{(U^3+9Ut^2)^2-(U^2+24t^2)^3}]^{1/3}. \tag{5}$$

The spin states of the two- and three-electron systems are singlet and doublet, respectively. It can be shown that all triplet states for the two-electron system and the quartet state for the three-electron system have higher energy than singlet and doublet states, respectively. Under the approximation of $U\gg t$, A is simplified as $U+\sqrt{6}|t|i$ and therefore $E(2)$ and $E(3)$ become

$$E(2)=-\sqrt{2}|t|, \quad E(3)=0, \tag{6}$$

respectively. The effective on-site Coulomb repulsion energy for the donor triad U_{eff} is then calculated as

$$U_{\text{eff}}\equiv E(1)+E(2)-2E(2)=\sqrt{2}|t|. \tag{7}$$

As a result, the transfer integral within the triad ($t=t_{\text{intra}}$) is 1.4 times more sensitive than the transfer integral between triads (t_{inter}) to the ratio $U_{\text{eff}}/t_{\text{inter}}$, which is an essential parameter for the strongly correlated electron system. Therefore, if t_{intra} increases faster than t_{inter} as the temperature decreases, the ratio $U_{\text{eff}}/t_{\text{inter}}$ is enhanced and therefore a Mott-type transition occurs. In the case of 1, the on-site Coulomb repulsion for isolated BEDT-TTF is greater than 1 eV, while the transfer integral within the triad (t_{qAA}) is about 0.19 eV at room temperature. The effective on-site Coulomb repulsion is then calculated as 0.27 eV. For the transfer integrals between the triads, the intracolumnar one (t_{qAB}) is 0.14 eV and the intercolumnar ones (t_{pAA}, t_{pAB}, t_{rAA}, t_{rAB}) are at most 0.07 eV. On lowering the temperature down to 105 K, both t_{qAA} and t_{qAB} are increased as 10%, while the change for the others is approximately 5% on average. This anisotropic change in the transfer integrals makes the ratio $U_{\text{eff}}/t_{\text{inter}}$ larger and, as a result, the transition from a semimetal to a Mott insulator is invoked. Since the disproportion within a column is not too large ($t_{qAB}/t_{qAA}\approx0.7$), we should treat an infinite alternate chain instead of an isolated trimer for further quantitative discussion. However, we can at least expect that the treatment developed above is qualitatively correct.

Finally, we summarize and compare the mechanism of the phase transition of HSO_4 salt (1) and ClO_4 salt (2). At room temperature these salts are isomorphic for the alignment of BEDT-TTF molecules. Both salts have a weakly trimerized columnar structure. As for counteranions, while ClO_4^- ions in 2 are rotated around one of the Cl–O bonds,[1] HSO_4 anions in 1 are dimerized via intermolecular cyclic hydrogen bonds and their rotation is totally suppressed. Their electronic structure is classified as a semimetal according to the energy band calculation, and the ESR and susceptibility results also support that there is no significant difference in their electronic structure in their metallic phase. On lowering the temperature, the cell parameters of both salts decrease significantly along the molecular stacking direction (the c axis), but the degree of anisotropy for 2 is larger than that for 1. This is presumably because the gradual quenching of anion rotation in 2 releases the steric hindrance along the stacking direction, whereas the rigidness of the cyclic anion dimer in 1 partially prevents the contraction along this direction. At 170 K donor molecules in 2 begin to change their orientation and the side-by-side overlap and transfer integral between molecules are reduced. This structural change is responsible for the semimetal–band-insulator transition of this salt. For the case of salt 1, instead of such a structural change, the effective on-site Coulomb repulsion for the trimer unit becomes larger as a result of thermal contraction, which gives rise to semimetal–Mott-insulator transition at 126 K. We could say that, although the hydrogen bonds between anions do not play a principal role in the phase transition itself, they affect the rotational degree of freedom for anion sites, which makes the mechanism of the phase transition for 1 totally different from that for 2. In this sense, the nature of the phase transition for these materials is controlled by the existence of intermolecular hydrogen bonds between anions.

SUMMARY

$(BEDT\text{-}TTF)_3(HSO_4)_2$ is a two-dimensional molecular conductor and has a metal-insulator transition at 126 K. We investigate this transition by means of x-ray diffraction, electrical conductivity measurement, ESR, magnetic susceptibility measurement, thermal analyses, and deuterium substitution at counteranion or donor sites. There are cyclic hydrogen bonds between two counteranion molecules and one of the six-membered rings is disordered at room temperature, which is suppressed before the metal-insulator transition takes place. The transition turns out to be first order in nature, having a quite small enthalpy and entropy change at the transition point. The structural change associated with the

transition is undetectable and there is no noteworthy difference in its energy band structure between metallic and insulator phases. This discrepancy comes from the electron correlation whose existence is supported by the enhanced Pauli paramagnetic susceptibility. Using the triad unit model, the effective on-site Coulomb repulsion can be described in terms of intratrimer transfer integrals, which are enlarged by lattice contraction when temperature decreases. As a result, the mechanism of the metal-insulator transition is not a structural one, but rather described as a kind of Mott transition.

[1] T. Enoki, K. Tsujikawa, K. Suzuki, A. Uchida, Y. Ohashi, H. Yamakado, K. Yakushi, and G. Saito, Phys. Rev. B **50**, 16 287 (1994).

[2] N. D. Kush, V. N. Laukhin, A. I. Schegolev, E. B. Yagubskii, E. Yu, Alikberova, and R. S. Rukk, J. Phys. (France) I **1**, 1365 (1991).

[3] S. S. P. Parkin, E. M. Engler, V. Y. Lee, and R. R. Schumacker, Mol. Cryst. Liq. Cryst. **119**, 375 (1985).

[4] H. Kobayashi, R. Kato, T. Mori, A. Kobayashi, Y. Sasaki, G. Saito, T. Enoki, and H. Inokuchi, Chem. Lett., 179 (1984).

[5] L. C. Porter, H. H. Wang, M. M. Miller, and J. M. Williams, Acta Cryst. C **43**, 2201 (1987).

[6] A. Brandstrom, *Preparative Ion Pair Extraction*, 2nd ed. (Apotekarsocieteten/Hässle Läkemedel, Stockholm, 1976).

[7] G. M. Sheldrick, SHELXS86, program for crystal structure determination, University of Göttingen, Federal Republic of Germany, 1986.

[8] G. M. Sheldrick, SHELXL93, program for refinement of crystal structures, University of Göttingen, Federal Republic of Germany, 1993.

[9] T. Mori, A. Kobayashi, Y. Sasaki, H. Kobayashi, G. Saito, and H. Inokuchi, Bull. Chem. Soc. Jpn. **57**, 627 (1984).

[10] J. H. Ammeter, H.-B. Bürgi, J. Thibeault, and R. Hoffman, J. Am. Chem. Soc. **100**, 3686 (1978).

[11] Symmetry operations: (i) $x-1, y, z-1$; (ii) $-x, 1-y, 1-z$; (iii) $1-x, 1-y, 1-z$; (iv) $2-x, y, 1-z$; (v) $1-x, 1-y, 2-z$.

[12] M. Ichikawa, Acta Cryst. B **34**, 2074 (1978).

[13] S. Etemad, Phys. Rev. B **13**, 2254 (1978).

[14] S. S. P. Parkin, M. Miljak, and J. R. Cooper, Phys. Rev. B **34**, 1485 (1986).

[15] T. Enoki, K. Imaeda, M. Kobayashi, H. Inokuchi, and G. Saito, Phys. Rev. B **33**, 1553 (1986)

[16] T. Sugano, G. Saito, and M. Kinoshita, Phys. Rev. B **34**, 117 (1986). .

[17] G. A. Samara, Ferroelectrics **20**, 87 (1978), and references cited therein.

[18] Y. Ohashi, K. Yanagi, T. Kurihara, Y. Sasada, and Y. Ohgo, J. Am. Chem. Soc. **103**, 5805 (1981).

[19] R. Świetlik, N. D. Kushch, L. A. Kushch, and E. B. Yagubskii, Phys. Status Solidi B **181**, 499 (1994).